

# Quantification and localization of contrast agents using delta relaxation enhanced magnetic resonance at 1.5 T

Uvo Christoph Hoelscher · Steffen Lothar ·  
Florian Fidler · Martin Blaimer · Peter Jakob

Received: 9 August 2011 / Revised: 18 October 2011 / Accepted: 19 October 2011 / Published online: 27 November 2011  
© ESMRMB 2011

## Abstract

**Object** Delta relaxation enhanced magnetic resonance (dreMR) is a new imaging technique based on the idea of cycling the magnetic field  $B_0$  during an imaging sequence. The method determines the field dependency of the relaxation rate (relaxation dispersion  $dR_1/dB$ ). This quantity is of particular interest in contrast agent imaging because the parameter can be used to determine contrast agent concentrations and increases the ability to localize the contrast agent.

**Materials and methods** In this paper dreMR imaging was implemented on a clinical 1.5 T MR scanner combining conventional MR imaging with fast field-cycling. Two improvements to dreMR theory are presented describing the quantification of contrast agent concentrations from dreMR data and a correction for field-cycling with finite ramp times.

**Results** Experiments demonstrate the use of the extended theory and show the measurement of contrast agent concentrations with the dreMR method. A second experiment performs localization of a contrast agent with a significant improvement in comparison to conventional imaging.

**Conclusion** dreMR imaging has been extended by a method to quantify contrast agent concentrations and

improved for field-cycling with finite ramp times. Robust localization of contrast agents using dreMR imaging has been performed in a sample where conventional imaging delivers inconclusive results.

**Keywords** Contrast agent · Quantification · Localization · MRI

## Introduction

Many applications in MRI employ contrast agents to enhance the detection of medically important information such as tumors and lesions. However in most cases conventional imaging does not facilitate robust quantification and localization of contrast agents. The reason for this problem is that the detection of contrast agents relies on their ability to modify the relaxation rates of surrounding hydrogen protons. The contrast agent does not provide any intrinsic MR signal but alters the protons signal at its location. Hence contrast agents can only be detected indirectly in MR images by finding the change in the proton signal.

dreMR imaging [1] addresses this problem by modulating the relaxation rate ( $R_1$ ) of the contrast agent and consequently image intensity at locations with contrast agent. Subtraction of two modulated images highlights tissue with contrast agent and suppresses signals from tissue without contrast agent. The change of the relaxation rate is induced by cycling the  $B_0$  magnetic field during the imaging sequence. Therefore dreMR does not yield  $R_1$  contrast but displays the magnetic field dependence of the relaxation rate (relaxation dispersion  $dR_1/dB$ ). This quantity can be very high for tissue with contrast agent at a magnetic field strength of 1.5 T and is much smaller for

---

U. C. Hoelscher (✉) · S. Lothar · F. Fidler · M. Blaimer ·  
P. Jakob  
Research Center for Magnetic Resonance Bavaria (MRB),  
Würzburg, Germany  
e-mail: hoelscher@mr-bavaria.de

P. Jakob  
Department of Experimental Physics 5,  
University of Würzburg, Würzburg, Germany

tissue without contrast agent [1]. In addition relaxation dispersion is directly proportional to the concentration of the contrast agent in tissue/solvent [5]. dreMR images have the advantage of suppressing the anatomical background signal like e.g. PET or fluorine imaging but can easily be superposed to anatomical images.

Previous work by Alford et al. [1–3] employing the dreMR method demonstrated differentiation between bound and unbound contrast agents. Their experiments show an increase in image contrast for the contrast agent MS-325 bound to large biomolecules like proteins.

This work aims at expanding dreMR theory and exploring further benefits of dreMR imaging. One improvement to the theory is proposed to include the effect of finite ramp times and a settling time during the field-cycling. This correction will be of importance if the ramp times and the settling time are not negligibly short in comparison to the whole field-cycling process. A second extension to the theory is derived which allows to extract quantitative concentrations of contrast agents from dreMR data.

Two experiments demonstrate concentration and localization measurements of contrast agents. The first experiment performs concentration measurements which are based on the extended theory. The second experiment shows localization of a contrast agent in a biological sample where  $T_1$  weighted images deliver inconclusive results, but dreMR images clearly pinpoint the contrast agent.

## Materials and methods

The MR physical parameters of dreMR suitable contrast agents and the perspective to address biological and medical problems recommend the use of 1.5 T clinical scanners for dreMR experiments. However clinical scanners stand for restrictions like absolutely constant  $B_0$  field and fixed frequency in the detection chain which oppose the need to cycle the  $B_0$  magnetic field.

To overcome these limitations dreMR experiments use an insert field coil to add an additional homogeneous field  $\Delta B$  in superposition to the constant  $B_0$  field at specific times during the imaging sequence. This combination of MRI and fast field-cycling (FFC) has experienced little attention so far, but is promising for many new  $R_1$  specific applications [4, 6, 9]. The offset coil is placed at the isocenter of a scanner and superposes its field parallel or antiparallel to the  $B_0$  field. The imaging sequence is designed in a way that radio frequency (RF) transmitting and receiving always take place at times with  $\Delta B = 0$  and relaxation at times with  $\Delta B \neq 0$ . This scheme guarantees that standard RF equipment and gradients can be used for

imaging without the need for modification and spin relaxation can take place at fields  $B_0 \pm \Delta B$ .

Figure 1 shows a diagram of a dreMR sequence. Phase (1) is the preparation of the magnetization. It can comprise e.g. inversion and saturation pulses played out at  $B_0$ . Phases (2) to (4) represent the evolution period with the duration  $T_{evol}$ : (2) offset coil ramps the field quickly from  $B_0$  to  $B_0 \pm \Delta B$ , (3) the magnetic field is held at constant  $B_0 \pm \Delta B$  and magnetization relaxes with corresponding relaxation rate and (4) ramping the field quickly back to  $B_0$ . Phase (5) is a settling time which can be necessary if the system requires a short time between ramp end and image acquisition to stabilize. The last phase (6) is an imaging module. Here again the magnetic field is at constant  $B_0$  and all aspects of imaging can be executed with standard scanner hardware.

## Hardware and contrast agent

The main technical challenge of a dreMR experiment is the offset coil. For the experiments we use a home-built field-cycling coil shown in Fig. 2. The operation inside a clinical scanner requires precise active shielding to minimize stray fields. Field homogeneity is of minor importance as the coil is only used during times with the magnetization being parallel to the  $z$ -axis (so dephasing due to inhomogeneities cannot happen).

In our coil homogeneity across the imaging region (diameter of 34 mm, length of 50 mm) is better than 1% which is sufficient for dreMR imaging and does not require any correction. The coil has a resistance of 0.6  $\Omega$  and an inductance of 4.9 mH. It is operated at 37 A and has a field of  $\pm 90$  mT in its center. The weight of the coil is about 10 kg. It is water cooled to keep its temperature in a reasonable range. Due to design restrictions the overall cooling capacity limits the duty cycle to 1:8.

Active shielding is a necessity for the offset coil. All stray fields at radii greater than the inner wall of the scanner induce eddy currents in the cold bore and couple to

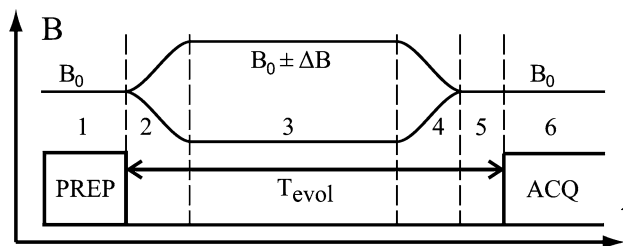


**Fig. 1** Diagram of dreMR experiment with phase 1 preparation, phase 2 ramp from  $B_0$  to  $B_0 \pm \Delta B$ , phase 3 constant field at  $B_0 \pm \Delta B$  with corresponding relaxation, phase 4 ramp from  $B_0 \pm \Delta B$  to  $B_0$ , phase 5 settling time and phase 6 image acquisition

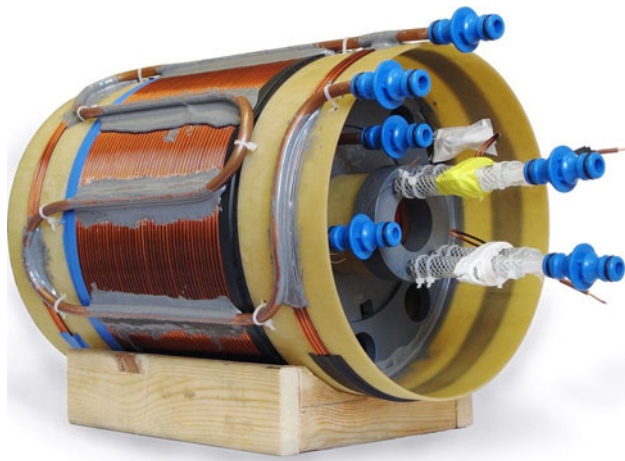


**Fig. 2** Water cooled fast field-cycling offset coil used for dreMR experiments. The coil is inserted into a clinical scanner to increase or decrease its  $B_0$  field by  $\pm 90$  mT. Outer windings are an active shielding coil, inner windings (not visible) produce the actual offset field

the superconducting coils. Therefore stray fields significantly decrease  $B_0$  stability and homogeneity and must be minimized. The coil uses a set of counter-windings at about three times the radius of the actual offset field coil to cancel the fringe field. They reduce the remaining field at a radius of 30 cm (radius of scanner bore) to values smaller than 15  $\mu$ T which is a reduction of a factor of approximately 35 in comparison to an unshielded coil.

Nevertheless the remaining stray fields induce  $B_0$  eddy currents in the scanner which change the Larmor frequency by up to  $\pm 60$  Hz and decay with a time constant of 250 ms. These changes in frequency are present during image acquisition and have to be compensated for. We have implemented a sequence which dynamically adjusts the RF transmitting and receiving frequency of the scanner to prevent a dislocation of the image in read and slice direction.

The active shielding fulfills a second important task. Forces and torques on magnetic objects can be very strong in 1.5 T scanners. The placement of the unshielded offset coil at the isocenter of the scanner should prevent any net forces or torques, but even small misalignments can cause a dangerous acceleration of the coil. The shielding of the offset coil reduces the forces and torques significantly such that even misalignments up to 5 cm or  $10^\circ$  can be tolerated.

Figure 2 shows a photo of the offset coil. The outer windings in the image are the active shielding coil with cooling pipes attached, the actual offset field coil is in its center and not visible. The coil is driven by a home-built power supply which can play out bipolar currents. Ramp times for the offset coil are  $\leq 8$  ms for ramp up and  $\leq 4$  ms for ramp down. Within the offset coil a home-built shielded

RF birdcage coil is used for RF transmitting and receiving. Its imaging region has a diameter of 34 mm and a length of 70 mm.

For now most promising substances for dreMR imaging at 1.5 T have been found in the family of Gadolinium (Gd) based contrast agents. In general the best suited contrast agents have a very high relaxation dispersion. The relaxation rate  $R_1$  is the product of the contrast agent concentration  $c$  and the relaxivity  $r_1$  ( $R_1 = c \cdot r_1$ ). All images presented in this paper were acquired with Gadofluorine M (Schering, LOT N2044 A01) which has a sufficient high relaxation dispersion.

## Theory

dreMR experiments are based on subtracting two images in which the magnetization has evolved with increased and decreased  $B_0$  field. All substances with non-vanishing field dependence of their relaxation rate like e.g. contrast agents yield different intensities in the two images and hence have remaining signal after subtraction. Pure tissue, which has a very low relaxation dispersion, has almost equal intensities in both images such that its signal is strongly suppressed after subtraction.

The signal strength in MR images is proportional to  $M_0 \propto |B_0|$ . Therefore cycling the  $B_0$  field has two effects: the desired change in relaxation rate and a change in overall signal strength.

### dreMR image intensity

A detailed derivation of signal strength in a dreMR experiment is given in [1] and summarized in excerpts below as far as needed for the advancement of the theory.

One image with increased and one image with decreased  $B_0$  field are acquired following the scheme from Fig. 1 with a saturation as preparation. Their image intensities read (the subscript  $\pm$  indicates positive or negative  $\Delta B$  field)

$$S(T_{\text{evol}})_{\pm} \propto M_0 \frac{B_0 \pm \Delta B}{B_0} \left[ 1 - e^{-(R_1 \pm \Delta B R_d) T_{\text{evol}}} \right] \quad (1)$$

where  $T_{\text{evol}}$  is the total time for cycling the field  $\Delta B$  including ramp times and settling time (compare Fig. 1),  $R_1$  is the relaxation rate at 1.5 T and  $R_d = dR_1/dB$  the relaxation dispersion. The proportionality symbol accounts for a constant scaling factor between magnetization and signal strength which depends on hardware and readout sequence. For the sake of simplicity this constant subsequently is set to unity.

A normalization removes the influence of the changing equilibrium magnetization  $M_0(B_0)$  on the image intensities  $S(T_{\text{evol}})_{\pm}$

$$S(T_{\text{evol}})_{\pm,n} = \frac{B_0}{B_0 \pm \Delta B} \cdot S(T_{\text{evol}})_{\pm} \\ = M_0 \left[ 1 - e^{-(R_1 \pm \Delta B R_d) T_{\text{evol}}} \right] \quad (2)$$

where the index  $n$  indicates the normalized values. After subtraction of  $S(T_{\text{evol}})_{+,n}$  and  $S(T_{\text{evol}})_{-,n}$  the signal intensity is

$$I(T_{\text{evol}}) = \sqrt{2} (M_0 e^{-R_1 T_{\text{evol}}}) \sinh(\Delta B_{\text{eff}} R_d T_{\text{evol}}). \quad (3)$$

This formula is similar to the one presented in [1] but has been modified in two ways: A factor of  $\sqrt{1/2}$  has been added in the subtraction to have equal noise levels in the acquired images  $S(T_{\text{evol}})_{\pm}$  and the subtraction image  $I(T_{\text{evol}})$ . This factor simplifies the comparison of image quality of acquired and processed images. Secondly the applied offset field  $\Delta B$  has been replaced by an effective offset field  $\Delta B_{\text{eff}}$  which accounts for finite ramp times.

#### Effective offset field and signal maximum

An exact mathematical expression for the effective offset field  $\Delta B_{\text{eff}}$  can only be given as integral, therefore an approximation is proposed. The linear ramps (2) and (4) from Fig. 1 are replaced by step functions played out after half the ramp duration. As result the shape of the offset field in time changes from a trapezoid with duration  $t_2 + t_3 + t_4$  to a rectangular function with duration  $t_2/2 + t_3 + t_4/2$  (times  $t_2$  to  $t_4$  correspond to the durations of the phases 2–4 in Fig. 1). This choice assumes that the error due to the missing field in the one half of the step function is compensated by the error due to the overvalued field in the other half. For ramp times much shorter than the  $T_1$  values of the sample, this is a good assumption. The effective field is given by the ratio of these two durations. Furthermore a correction for the settling time  $t_5$  is added. During this time the magnetization relaxes with the relaxation rate  $R_1$  at 1.5 T against the equilibrium magnetization  $M_0$  at 1.5 T. The magnetization converges against the dynamics for a magnetization which has not experienced an offset field. Hence the settling time reduces the effective offset field. The degree to which the magnetization has relaxed against the equilibrium magnetization at the beginning of the settling time is important; therefore the previous evolution has to be taken into account. The behavior is modeled by an exponential decay with the decay constant being depended on the evolution time. To obtain the term the ratio between a magnetization with and a magnetization without the offset field has been calculated and approximated for settling times much shorter than  $T_1$

$$\Delta B_{\text{eff}} = \Delta B \left[ \frac{t_3 + \frac{t_2+t_4}{2}}{t_2 + t_3 + t_4} \right] \cdot e^{-R_1 t_5}. \quad (4)$$

$\Delta B$  is the offset field amplitude during the phase of constant field. The decay constant  $R_1'$  decreases the effective offset field  $\Delta B_{\text{eff}}$  according to the duration of the settling time  $t_5$ . It reads  $R_1' = R_1 \cdot (1 - e^{-R_1 T_{\text{evol}}})^{-1}$  and is—as mentioned before—dependent on the previous evolution of the magnetization. The value of  $R_1'$  is always larger than  $R_1$  but approaches  $R_1$  for evolution times much longer than the relaxation time. From now on the offset field  $\Delta B$  will always be replaced by the effective field  $\Delta B_{\text{eff}}$ .

To verify the proposed approximation, the Bloch equations have been numerically integrated to find the dynamics of the magnetization during the evolution time  $T_{\text{evol}}$ . The time behavior of the magnetic field  $B(t) = B_0 + \Delta B(t)$  has been modeled like in Fig. 1. For the simulation ramp up times of 8 ms and ramp down times of 4 ms have been used (like achieved with our setup); the settling time  $t_5$  is 10 ms. The constant offset field between the ramps was 90 mT; a material with no relaxation dispersion and a relaxation time  $T_1 = 350$  ms was used.

dreMR as a subtractive imaging method suffers from a poor signal to noise ratio, therefore maximizing the dreMR signal is of great importance. For using optimal experiment parameters the maximum of Eq. 3 has been determined. The solution is

$$T_{\text{evol,max}} = \frac{1}{\Delta B_{\text{eff}} R_d} \operatorname{atanh} \left( \frac{\Delta B_{\text{eff}} R_d}{R_1} \right) \approx (R_1)^{-1}. \quad (5)$$

Usually  $|\Delta B_{\text{eff}} R_d| \ll R_1$  such that the inverse hyperbolic tangent in Eq. 5 can be approximated by its first linear term of the Taylor series. For the used contrast agent the ratio is  $|\Delta B_{\text{eff}} R_d|/R_1 = 0.025$  resulting in an error  $\ll 1\%$ . This choice of  $T_{\text{evol}}$  maximizes the dreMR signal  $I(T_{\text{evol}})$  independently of applied offset field  $\Delta B$  and relaxation dispersion  $R_d$  and hence yields the best SNR.

#### Concentration determination

The relaxation dispersion of a contrast agent is a linear function of the concentration of the contrast agent in tissue/solvent

$$R_d = \left. \frac{dR_1}{dB} \right|_{1.5T} = c \cdot r_d \quad (6)$$

where  $c$  is the concentration and  $r_d$  the relaxivity dispersion. This fact can be exploited for retrieving the concentration of a contrast agent from a dreMR experiment. The relaxation dispersion  $R_d$  in Eq. 3 can be substituted by the term above

$$I(T_{\text{evol}}) = \sqrt{2} (M_0 e^{-R_1 T_{\text{evol}}}) \sinh(\Delta B_{\text{eff}} (c \cdot r_d) T_{\text{evol}}). \quad (7)$$

This equation can now be solved for the concentration  $c$ . However the relaxation rate  $R_1$  occurring in the factor

$(M_0 e^{-R_1 T_{\text{evol}}})$  still is unknown. The term can be eliminated from the equation by a substitution with the two acquired images from increased and decreased field. They have been normalized and subtracted to find Eq. 3. When adding the two normalized images  $S(T_{\text{evol}})_{\pm,n}$

$$S(T_{\text{evol}})_{+,n} + S(T_{\text{evol}})_{-,n} = M_0 \left[ \left( 1 - e^{-(R_1 + \Delta B_{\text{eff}} R_d) T_{\text{evol}}} \right) + \left( 1 - e^{-(R_1 - \Delta B_{\text{eff}} R_d) T_{\text{evol}}} \right) \right] \tag{8}$$

rearranging leads to a substitution for the factor  $(M_0 e^{-R_1 T_{\text{evol}}})$  which reads

$$(M_0 e^{-R_1 T_{\text{evol}}}) = \frac{2M_0 - (S(T_{\text{evol}})_{+,n} + S(T_{\text{evol}})_{-,n})}{2 \cosh(\Delta B_{\text{eff}} R_d T_{\text{evol}})} \tag{9}$$

Combining Eqs. 7 and 9 and rearranging leads to

$$\tanh(\Delta B_{\text{eff}} (c \cdot r_d) T_{\text{evol}}) = \frac{\sqrt{2} I(T_{\text{evol}})}{(2M_0 - (S(T_{\text{evol}})_{+,n} + S(T_{\text{evol}})_{-,n}))} \tag{10}$$

This equation is suited for the measurement of the concentration  $c$ , because it only comprises the normalized images  $S(T_{\text{evol}})_{\pm,n}$ , a proton density weighted image  $M_0$  (at  $B_0$ ), the sequence parameters  $\Delta B_{\text{eff}}$  and  $T_{\text{evol}}$  and the relaxivity dispersion  $r_d$ .

The value of  $r_d$  has to be determined in a separate experiment and can be used for subsequent concentration measurements in the same tissue or solvent. After this has been done all concentration measurements require the two images with increased and decreased field and an image with proton density weighting at  $B_0$ .

Rearranging Eq. 10 leads to the concentration function  $C(T_{\text{evol}})$

$$C(T_{\text{evol}}) = c \cdot T_{\text{evol}} = \text{atanh} \left( \frac{\sqrt{2} I(T_{\text{evol}})}{(2M_0 - (S(T_{\text{evol}})_{+,n} + S(T_{\text{evol}})_{-,n}))} \right) \times \frac{1}{\Delta B_{\text{eff}} \cdot r_d} \tag{11}$$

If using the contrast agent Gadofluorine M and an offset field of 90 mT, the hyperbolic tangent in Eq. 11 can be approximated by a Taylor series. The condition  $(\Delta B_{\text{eff}} (c \cdot r_d) T_{\text{evol}} \ll 1)$  is well met for all reasonable evolution times. The concentration function  $C(T_{\text{evol}})$  now reads

$$C(T_{\text{evol}}) = c \cdot T_{\text{evol}} \approx \frac{\sqrt{2} I(T_{\text{evol}})}{(2M_0 - (S(T_{\text{evol}})_{+,n} + S(T_{\text{evol}})_{-,n}))} (\Delta B_{\text{eff}} \cdot r_d) \tag{12}$$

## Results

### Effective offset field

The Bloch equations have been numerically integrated to verify the proposed approximation of the effective field. These simulations yield the dynamics of the magnetization during the evolution time  $T_{\text{evol}}$ .

At several evolution times  $T_{\text{evol}}$  between 20 ms and 350 ms the magnetization has been determined at the moment of image acquisition with and without applied offset field. The difference between these values represents the total influence of the field-cycling. For infinitely short ramp times and a vanishing settling time the ratio of the two values would be exactly the ratio between  $B_0 \pm \Delta B$  and  $B_0$ . However for finite ramp and settling times the ratio between magnetization with and without applied offset field decreases. Therefore  $\Delta B$  has to be replaced by  $\Delta B_{\text{eff}}$  which is always smaller than  $\Delta B$ . Figure 3 shows the results for the simulation: The effective offset field  $\Delta B_{\text{eff}}$  is shown as circles and the dashed line represents the applied offset field  $\Delta B$ . The solid line indicates the given approximation from Eq. 4. For short evolution times the effective field diverges strongly from the applied field.

### Quantification

The concentrations of Gadofluorine M (Schering, LOT N2044 A01) samples in a dilution series were determined using dreMR imaging. At first the constant  $r_d$  of the used contrast agent was measured with multiple saturation recovery dreMR images. Its value for a magnetic field strength of 1.5 T and a temperature of 25°C is  $r_d = (-5.5 \pm 0.3) (\text{mMTs})^{-1}$  (corresponding to a change in

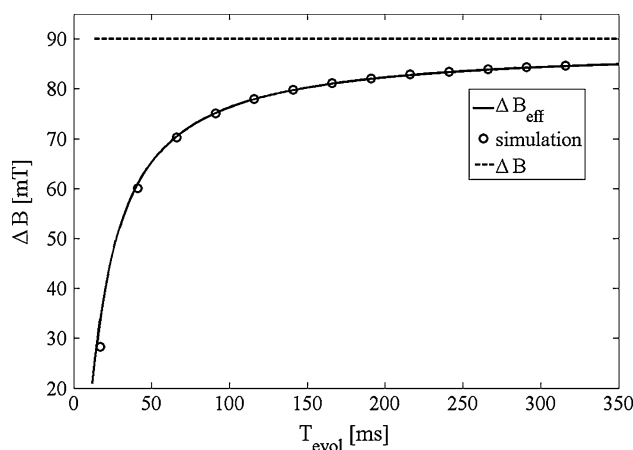


**Fig. 3** Simulation for the effective field  $\Delta B_{\text{eff}}$  with an offset field of  $\Delta B = 90$  mT: circles represent Bloch equation simulation, the solid line represents the approximation from Eq. 4 and the dashed line stands for the applied offset field  $\Delta B$

relaxivity of  $\Delta r_1 = -0.50 \text{ (mMs)}^{-1}$  for an offset field of 90 mT). This value was then used for all subsequent evaluations. The relaxivity of the contrast agent (for the same temperature and field strength) is  $r_1 = (15.7 \pm 0.5) \text{ (mMs)}^{-1}$ .

For the actual concentration measurement, dreMR images of a phantom containing three different concentrations of Gadofluorine M in NaCl were acquired. The phantom additionally comprised a reference sample with no relaxation dispersion which mimics tissue with a long  $T_1$ . Figure 4a shows a  $T_1$  weighted image of the phantom with the reference sample and the three Gadofluorine M samples from left to right. Concentrations for Gadofluorine M were: sample A 115  $\mu\text{M}$ , sample B 135  $\mu\text{M}$  and sample C 181  $\mu\text{M}$ . Part (b) of Fig. 4 shows the corresponding dreMR image. The reference sample does not yield any signal as its relaxation dispersion is zero.

In total four dreMR images were acquired with identical imaging parameters but different evolution times  $T_{\text{evol}}$  of 70, 150, 200 and 250 ms (imaging parameters:  $FOV = 23 \times 61 \text{ mm}^2$ , matrix size  $32 \times 80$ ,  $TE = 8.6 \text{ ms}$ ,  $TR = 3000 \text{ ms}$ , bandwidth 250 Hz/px, 8 averages). Exemplarily the dreMR image with  $T_{\text{evol}} = 150 \text{ ms}$  is shown in Fig. 4b. An additional scan (no offset field, short  $TE$ , sufficient long  $TR$ ) delivered the  $M_0$  data required in Eq. 11. Intensities of all Gadofluorine M samples were processed following Eq. 11 and plotted as function of evolution time  $T_{\text{evol}}$ . The result is displayed in Fig. 5. Data points follow the linear function  $C(T_{\text{evol}})$  from Eq. 12 with their slopes being the Gadofluorine M concentrations  $c$ . Table 1 compares known concentrations from sample preparation and concentrations measured via dreMR imaging. The errors for preparation concentrations are the imprecision accompanying the dilution process;

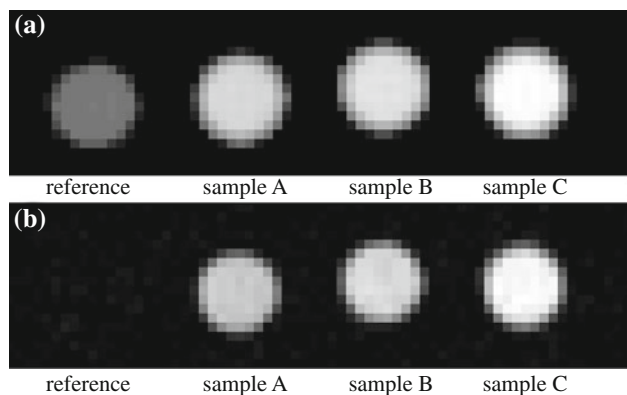


**Fig. 4** **a**  $T_1$  weighted image of concentration measurement phantom with (from left to right) reference sample (not relaxation dispersive) and three samples (A, B, C) with different concentrations of Gadofluorine M (relaxation dispersive). **b** Corresponding dreMR image with  $T_{\text{evol}} = 150 \text{ ms}$  where reference sample is black and Gadofluorine M samples are bright

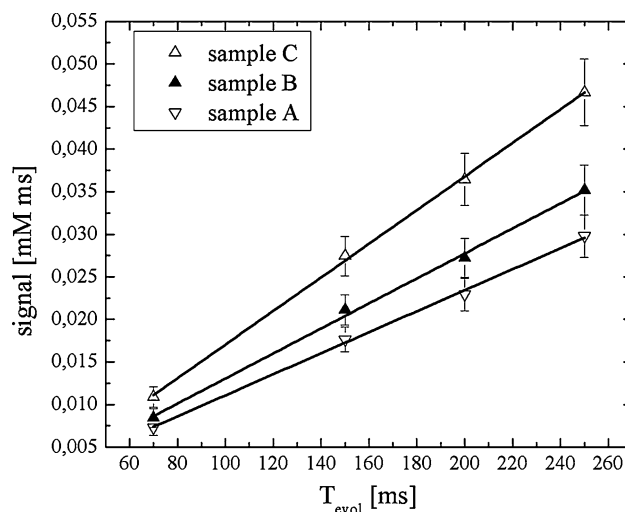


**Fig. 5** Plot of intensities for three Gadofluorine M samples (A, B, C) measured with four different evolution times  $T_{\text{evol}} = 70, 150, 200$  and  $250 \text{ ms}$ . The slopes of the linear fits  $C(T_{\text{evol}})$  (compare Eq. 11) are the concentrations  $c$  of the samples. The unusual unit of the signal [mM ms] is the product of the units of evolution time  $T_{\text{evol}}$  and concentration  $c$

errors for the measured concentrations come from the fit of the slope.

#### Localization

A solution of Gadofluorine M in NaCl with a concentration of 174  $\mu\text{M}$  was injected into a small area of a biological phantom (raspberry). The region of injected contrast agent is marked on a high resolution,  $T_1$  weighted turbo spin echo image (at 1.5 T) in Fig. 6a with a black ellipse. The image  $S(T_{\text{evol}})$  with decreased  $B_0$  field for generation of the dreMR image is shown in part (b). The corresponding dreMR image is shown in part (c). The fourth image (d) is a colored overlay of the dreMR image and the  $T_1$  weighted, high resolution image; the matrix size of the dreMR image was zero filled to match the size of image (a).

The dreMR image was generated from two spin echo images with an in-plane resolution of 520  $\mu\text{m}$ , a slice thickness of 2 mm and an echo time  $TE$  of 9.9 ms. The matrix size was  $42 \times 48$  data points for phase and read encoding respectively. Saturation was used for preparation followed by an evolution period with a duration  $T_{\text{evol}}$  of 340 ms and an offset field strength  $\Delta B$  of  $\pm 90 \text{ mT}$ . dreMR contrast is maximized for  $T_{\text{evol}} = 1/R_1$ ; hence the chosen  $T_{\text{evol}}$  matched the relaxation rate of the injected contrast agent (contrast agent concentration  $c = 174 \mu\text{M}$  corresponds to a  $T_1 \approx 340 \text{ ms}$ ).

24 averages were acquired to obtain a sufficient SNR. The total acquisition time was 90 minutes. Limiting factor was the thermal duty cycle of the offset coil which required a repetition time  $TR$  of 2700 ms ( $TR/T_{\text{evol}} = 7.7$ ). K-space

**Table 1** Comparison of concentrations of three Gadofluorine M samples

	Sample A	Sample B	Sample C
Prepared ( $\mu\text{M}$ )	$115 \pm 5$	$135 \pm 5$	$181 \pm 5$
Measured ( $\mu\text{M}$ )	$123 \pm 15$	$147 \pm 15$	$197 \pm 20$

The upper row displays known values from sample preparation, the lower row calculated values from dreMR imaging

lines of the two images were acquired in an interleaved fashion to reduce systematic errors.

## Discussion

The use of the proposed effective offset field  $\Delta B_{\text{eff}}$  is crucial to the evaluation of dreMR images. Normalization of the two acquired images with in- and decreased field depends on the exact knowledge of the offset field (compare Eq. 2). Even small errors in the value of the offset field lead to imperfect normalization and hence lower the quality of the suppression of non-dispersive materials. Figure 3 comparing the applied offset field  $\Delta B$  and the simulated data for  $\Delta B_{\text{eff}}$  clearly shows a divergence. Using the approximation given in Eq. 4 significantly improves the normalization and minimizes errors in the evaluation of dreMR data. All dreMR evaluations in this paper have used the effective offset field; the quantification would have been impossible without the correction.

A measurement of contrast agent concentrations using the dreMR method is presented. It yields values in agreement with sample preparation concentrations. The reference sample does not show any signal in the dreMR images and therefore clearly can be identified to be without relaxation dispersive contrast agent. For all Gadofluorine M samples, concentrations can be derived from dreMR data. One dreMR image  $I(T_{\text{evol}})$  should be sufficient for

concentration determination because Eq. 12 is a line through the origin and its slope can be found from a single data point. However Fig. 5 shows that the linear fits do not perfectly intersect at the origin. This behavior is caused by a non-perfect saturation in phase (1) of the dreMR experiment and can add a small positive or negative constant value to all data points in Fig. 5. For this reason the experiment comprises four measurements at different evolution times  $T_{\text{evol}}$  such that the slope can be determined from the data points without the use of the origin. The error of the measurement is influenced by two mechanisms: All images suffer from noise and artifacts. These errors can vary from sample to sample and from image to image. They propagate into the concentration error without systematic behavior. The second error mechanism is based on uncertainties in the relaxivity dispersion and the applied offset field strength. Errors in these quantities propagate systematically into the results. In the presented data in Table 1 all values are too large. It is likely that this behavior results from a too small value for the offset field and/or relaxivity dispersion as the concentration is inversely proportional to these values ( $c \propto 1/(r_d \Delta B)$ ). One reason for the error is the fact that the offset current is voltage controlled and therefore reduces with thermal heating in the offset coil.

Conventional concentration measurements using the linearity between relaxation rate  $R_1$  and the concentration  $c$  ( $R_{1,\text{meas}} = R_{1,\text{tis}} + c \cdot r_1$ ) require to know the relaxation rate of the tissue or solvent and the relaxivity of the contrast agent. The tissue relaxation rate usually is determined in a pre-contrast measurement [7]. dreMR experiments do not require the pre-contrast information on the relaxation rate of the tissue or solvent. They only depend on the relaxivity dispersion  $r_d$  of the contrast agent which can be measured in a separate experiment. It should be noted that both relaxivity and relaxivity dispersion of contrast agents often depend on their chemical environment. Therefore the

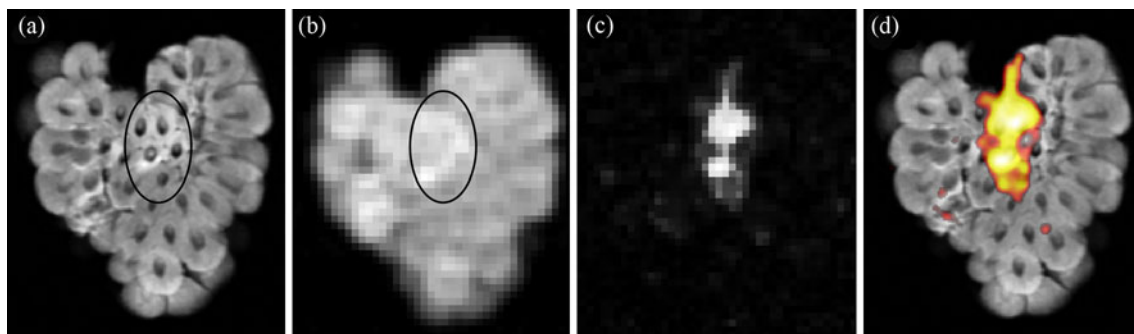


**Fig. 6** **a**  $T_1$  weighted, high resolution image of raspberry, Gadofluorine M was injected into the marked area; **b**  $T_1$  weighted image  $S(T_{\text{evol}})$  with decreased  $B_0$  field, injection marked; **c** corresponding dreMR image  $I(T_{\text{evol}})$ , regions with relaxation dispersive contrast

agent are bright and regions with non-dispersive fruit flesh are black; **d**  $T_1$  weighted image with a colored overlay of the dreMR image (zero filled)

conventional and dreMR imaging rely on knowing  $r_1$  or  $r_d$ , respectively, for the specific use. The dreMR method has the advantage that it requires just one parameter which can be measured either before or after the actual experiment. In comparison the conventional method requires two parameters including a post-contrast information. This fact is a great benefit for all experiments with long times between contrast agent administration and image acquisition like e.g. molecular imaging. If multiple measurements of the same tissue are carried out, it is possible to determine  $r_d$  just once and use the value for all concentration measurements in this chemical environment.

The goal of contrast agent imaging is to create a signal difference between tissue with and without contrast agent such that both regions can be visually distinguished. In samples with homogeneous tissue, this task can be performed if the signal difference between the regions is large in comparison to the noise (contrast to noise ratio  $CNR \gg 1$ ). For heterogeneous samples—like most biological samples—the spatial variations in spin density and relaxation rate in pure tissue can cause signal variations which are much larger than the noise. In this case the contrast agent signal gain has to be much larger than these variations for unambiguous localization. The  $T_1$  weighted image in Fig. 6b shows that signal increase due to contrast agent is not significantly larger than the variations in the regions without contrast agent.

The dreMR image in Fig. 6c has the advantage that the heterogeneous background signal is eliminated. Contrast agent signal has only to be compared against the noise; signal from the heterogeneous tissue without contrast agent vanishes. Due to this fact dreMR imaging provides a much better discrimination between tissue with and without contrast agent than conventional images.

Conventional contrast agent imaging can achieve similar suppression of pure tissue if a pre- and a post-contrast image are subtracted. However in practice this method proves tedious and is subject to many systematic errors like e.g. small changes in position,  $B_0$  field drifts, temperature drifts and diffusion processes. For a single image these effects usually do not lead to noticeable artifacts, but if two images are subtracted even small differences will cause severe changes in outcome and give rise to misinterpretation. Time spans between pre- and post-contrast image can be on the order of many hours or even days making proper subtraction very challenging or often impossible.

dreMR experiments acquire both images almost simultaneously. K-space lines are measured in an interleaved scheme such that the temporal delay between two equal k-space lines is just the repetition time  $TR$  which is on the order of a few seconds or below. All effects taking place on long time scales influence both images in the same way and do not lead to artifacts at the level of subtraction. This

circumstance makes dreMR contrast imaging robust and minimizes systematic errors.

For the setup used here measuring times for localization and concentration experiments so far are too long for clinical use. A first efficient step for scan time reduction will be a better cooling of the offset coil. If thermal dissipation no longer determines the repetition time  $TR$  the total scan duration can decrease by a factor of seven. Higher offset fields, fast and SNR effective imaging modules and techniques like compressed sensing can provide further decrease in acquisition time and will make dreMR contrast imaging possible within reasonable scan times. Alford et al. [3] have already shown first in vivo measurements supporting this prognosis.

In the experiments described the concentrations of the contrast agents are in a typical range for biological and medical MR imaging and therefore reflect reality of today's contrast agent applications. The improved discrimination between tissue with and without contrast agent observed in the localization measurement gives rise to the expectation that dreMR imaging can lower the detection level of contrast agents. For imaging of animal and human tissue, the influence of paramagnetic ions has to be investigated. These ions occur in some organs like e.g. the liver and can cause a relaxation dispersion in tissue leading to a background signal [8].

Many applications can benefit from dreMR measurements to a high degree. Especially molecular and cellular imaging usually use contrast agents for detection, but often require long times for contrast agent accumulation or intend to observe the temporal development of a process. dreMR measurements promise to overcome many temporal problems arising from the long time scales and to allow for measurements with lower concentrations.

In future experiments we will improve the hardware and apply this technique to small animal imaging. We expect this method to expand application fields for contrast agents.

## Conclusion

In this work, we have expanded the dreMR theory to quantitative concentration measurements and proposed a correction to the theory to include effects of finite ramp times during the field-cycling. We demonstrated profound quantification and localization with dreMR imaging at 1.5 T in a clinical scanner. This mechanism exclusively provides signal at locations with contrast agent and suppresses pure tissue. Its data can be used for exact quantification of concentrations. The dreMR image allows clear differentiation between tissue with and without contrast agent whereas a conventional image suffers from a heterogeneous background masking the contrast agent signal.



**Acknowledgments** This work was performed with support from the Federal Ministry of Education and Research under Award No 01EZ0816, Siemens Healthcare Sector Erlangen and the Bavarian Ministry of Economic Affairs, Infrastructure, Transport and Technology. We thank Gunthard Lykowsky for his support with the RF birdcage coil and Philipp Kagerbauer for sample preparation.

## References

1. Alford JK, Rutt BK, Scholl TJ, Handler WB, Chronik BA (2009) Delta relaxation enhanced MR: improving activation-specificity of molecular probes through R1 dispersion imaging. *Magn Reson Med* 61(4):796–802
2. Alford JK, Farrar CT, Yang Y, Handler WB, Chronik BA, Scholl TJ, Madan G, Caravan P (2011) Direct albumin imaging in mouse tumour model. *Proc Intl Soc Mag Reson Med* 19:318
3. Alford JK, Sorensen AG, Benner T, Chronik BA, Handler WB, Scholl TJ, Madan G, Caravan P (2011) Direct protein imaging of inflammation in the human hand. *Proc Intl Soc Mag Reson Med* 19:452
4. Hoelscher U, Lothar S, Fidler F, Blaimer M, Jakob P (2010) Unambiguous localization of contrast agents via B0-field-cycling. *Proc Intl Soc Mag Reson Med* 18:4939
5. Landis CS, Li X, Telang FW, Coderre JA, Micca PL, Rooney WD, Latour LL, Vetek G, Palyka I, Springer CS (2000) Determination of the mri contrast agent concentration time course in vivo following bolus injection: Effect of equilibrium transcytolemmal water exchange. *Magn Reson Med* 44(4):563–574
6. Lurie DJ, Aime S, Baroni S, Booth NA, Broche LM, Choi CH, Davies GR, Ismail S, O Hogain D, Pine KJ (2010) Fast field-cycling magnetic resonance imaging. *C R Phys* 11(2):136–148
7. Makowski MR, Wiethoff AJ, Jansen CH, Botnar RM (2009) Molecular imaging with targeted contrast agents. *Top Magn Reson Imag* 20(4):247–259
8. Negendank W, Corbett T, Crowley M, Kellogg C (1991) Evidence for a contribution of paramagnetic ions to water proton spin-lattice relaxation in normal and malignant mouse tissues. *Magn Reson Med* 18(2):280–293
9. Ungersma SE, Matter NI, Hardy JW, Venook RD, Macovski A, Conolly SM, Scott GC (2006) Magnetic resonance imaging with T1 dispersion contrast. *Magn Reson Med* 55(6):1362–1371